The ECM-backbone of the Lang-Kobayashi equations: a geometric picture

Vivi Rottschäfer
Mathematical Institute
Leiden University
P.O. Box 9512
2300 RA Leiden
The Netherlands
vivi@math.leidenuniv.nl

Bernd Krauskopf
Engineering Mathematics
University of Bristol
University Walk
Bristol BS8 1TR
United Kingdom
B.Krauskopf@bristol.ac.uk

October 2005

Abstract

We perform an analytical study of the external cavity modes of a semiconductor laser subject to conventional optical feedback as modeled by the well-known Lang-Kobayashi equations. Specifically, the bifurcation set is derived in the three-dimensional parameter space of feedback phase, feedback strength and pump current of the laser. Different open regions in this space correspond to different numbers of physically relevant external cavity modes of the laser. Some of their stability properties are determined from the characteristic equation.

Keywords:
Laser with optical feedback, external cavity modes, bifurcation set.

1 Introduction

Semiconductor lasers are the lasers of choice in many technological applications, ranging from optical storage to optical telecommunication. In such systems reflections from other components are generally unavoidable. In essence some of its light re-enters the laser after a certain delay time, which is due to the travel time of the light outside of the laser; see, for example, [Krauskopf and Lenstra (2005), Kane and Shore (2005)] as entry points to the extensive literature on lasers with optical feedback. Relative to the fast internal time scales of semiconductor lasers, this delay time is typically large and cannot be neglected. It is well-established that feedback of less than 1% can already totally destabilize the operation of a semiconductor laser. In this regime of operation, known as low frequency fluctuations, the laser typically switches off at irregular intervals. In

applications of semiconductor lasers it is often necessary to employ expensive optical isolators (that let the light pass in only one direction). On the other hand, chaotic laser light has been suggested for applications such as secure communication systems [Fischer et al. (2000b), Van Wiggeren and Roy (2002), Ohtsubo and Davis (2005)].

The prototypical example of a laser subject to delayed optical feedback is that of a single semiconductor laser receiving optical feedback from a conventional mirror positioned at some distance L away from the laser. One also speaks of the conventional optical feedback (COF) laser. This system has received considerable attention in recent years both experimentally and in terms of mathematical modelling; see the recent surveys [Van Tartwijk and Agrawal (1998), Fischer et al. (2000a), Gavrielides (2000), Krauskopf (2005)] as general references to the literature on the COF laser. Note that other types of delayed feedback, such as phase-conjugate feedback or filtered feedback, are also possible [Lenstra *et al.* (2005)], but here we concentrate solely on the COF laser.

We consider the *Lang-Kobayashi (LK) equations* — a well-established model of the COF laser [Lang and Kobayashi (1980)]. The LK equations describe the dynamics of the complex electric field $E = E_x + iE_y$ and the inversion (number of electron-hole pairs) N inside the laser. In numerous numerical studies they have been shown to describe experimental observations in considerable detail when two main modelling assumptions are satisfied, namely, that the feedback is quite weak (on the order of up to a few percent of the emitted light) and that the mirror is quite far away from the laser (on the order of several centimeters to meters). The LK equations can be written in non-dimensionalized form as

$$\begin{aligned} \tfrac{dE}{dt} &= \Big(1+i\alpha\Big)N(t)E(t) + \kappa e^{-iC_p}E(t-\tau), \\ T\tfrac{dN}{dt} &= P - N(t) - \Big(1+2N(t)\Big)|E(t)|^2. \end{aligned} \tag{1}$$

The parameters describing material properties of the laser are the ratio of decay times T and the linewidth-enhancement factor α. The parameter P is the pump current, that is, the amount of electrical energy supplied to the laser. In (1) the value $P = 0$ corresponds to the solitary laser threshold, that is, to the value of the pump current when the laser starts to switch on in the absence of optical feedback. Finally, there are three parameters that specify the optical feedback, namely the delay time τ, the feedback strength κ, and the feedback phase C_p. We remark that $C_p = \omega_0\tau$, where ω_0 is the optical frequency. Note that for sufficiently large τ the quantity C_p can be seen as an independent parameter; it can be changed, for example, by minuscule changes in the distance of the mirror to the laser (on the order of one optical wave length).

Throughout this paper we use in concrete numerical examples the parameter values as in [Heil *et al.* (2003)], namely

$$T = 1710, \quad \alpha = 5.0 \quad \text{and } \tau = 70,$$

while C_p, κ and P may vary. Note that for different values of T, τ and α the global picture retains its qualitative features.

The LK equations (1) are mathematically a system of delay differential equations (DDEs). Hence, their phase space is the infinite-dimensional space $C[-\tau, 0]$ of continuous functions with values in (E, N)-space. This inherent infinite-dimensional nature of the system makes its analysis quite complicated; see, for example, [Diekmann *et al.* 1995, Hale and Verduyn Lunel (1993), Verduyn Lunel and Krauskopf (2000)] for more background information.

In this paper we perform a detailed mathematical analysis of the so-called external cavity modes (ECMs) of Eqs. (1). The number of possible ECMs of a COF laser is known in the literature; see, e.g., [Van Tartwijk and Agrawal (1998)]. However, some of these ECMs may not be physically relevant if the pump current is too low. Our aim here is to develop a comprehensive geometric picture of the structure of the ECMs in dependence on the feedback phase C_p, the feedback strength κ and the pump current P. Specifically, we present the bifurcation set of the ECMs in the three-dimensional (C_p, κ, P)-space that divides the (C_p, κ, P)-space into regions with different numbers of physically relevant ECMs of the COF laser. Our analysis extends the known results on the number of (possible) ECMs in a concise way. Furthermore, we determine some stability properties of ECMs by means of a study of the characteristic equation.

2 The basic solution

The LK equations (1) have the basic solution $(E, N) = (0, P)$ for all choices of the other parameters. The change of stability of the basic solution corresponds to the laser threshold: when this basic solution is stable the laser is off, and when it is unstable the laser is on.

By computing a linear variational equation in the (E, N)-variables around $(0, P)$, its characteristic equation is determined as

$$\left(\lambda + \frac{1}{T}\right)\left[\left(\lambda - P - e^{-\lambda\tau}\kappa\cos(C_p)\right)^2 + \left(\alpha P - e^{-\lambda\tau}\kappa\sin(C_p)\right)^2\right] = 0. \tag{2}$$

Introducing $\lambda = \nu + i\mu$ in (2), for $\kappa > 0$ and $T > 0$, and splitting the resulting equation into its real and complex parts reveals, after some manipulations, that the basic solution $(0, P)$ undergoes a Hopf bifurcation for

$$C_p^{H\pm}(\kappa, P) = \pm\left[\arccos\left(-\frac{P}{\kappa}\right) + \tau\sqrt{\kappa^2 - P^2}\right] - \alpha\tau P + 2k\pi. \tag{3}$$

Since $C_p^{H\pm}(\kappa, P)$ must be real, a Hopf bifurcation can only take place for $\kappa \geq P$.

Note that $C_p^{H\pm}(\kappa, P)$ forms one smooth two-dimensional surface in (C_p, κ, P)-space (for fixed k). When looking at cross sections for fixed P the resulting curves in the (C_p, κ)-plane change as P is varied. The curves change qualitatively at $P = \frac{1}{\tau}$. In summary, the basic solution $(0, P)$ generally loses its stability at $P = 0$. However, it is stable in a small closed region for $\kappa > 0$ and $0 < P < \frac{1}{\tau}$; see Fig. 1.

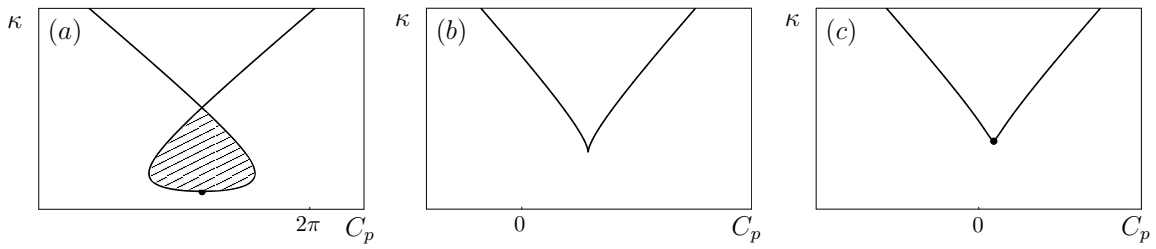

Figure 1: The curves $C_p^{H\pm}$ plotted for $0 < P < \frac{1}{\tau}$ (a), $P = \frac{1}{\tau}$ (b), and $P > \frac{1}{\tau}$ (c). In the shaded area in (a) the basic solution $(0, P)$ is stable, and everywhere else it is unstable. The minimum of the curve is always at $\kappa = P$ and C_p is shown over a 2π-wide interval.

3 Equations for ECMs

An ECM is also referred to in the literature as a continuous wave solution or a CW-state. It is a solution with constant intensity and inversion and a phase that depends linearly on time. In other words, it is of the form

$$E(t) = R_s e^{i\omega t} \quad \text{and} \quad N(t) = N_s\,, \tag{4}$$

where R_s, ω and N_s are constant. Mathematically, an ECM is a periodic orbit in (E, N)-space. It is important to realize that the ECMs are nevertheless the most simple solutions of Eqs. (1) apart from the basic solution, because the LK equations are invariant under the continuous symmetry group of all rotations of the complex E-plane. In fact, each ECM is a group orbit of this continuous symmetry, which means that in projection onto the (R, N)-space it is a single point; see [Krauskopf *et al.* (2000)]. For this reason ECMs are sometimes referred to as steady state solutions.

To find the ECMs one writes Eqs. (1) in polar coordinates by substituting $E(t) = R(t)e^{i\phi(t)}$, which gives

$$\begin{aligned} \tfrac{dR}{dt} &= N(t)R(t) + \kappa R(t-\tau)\cos\left(\phi(t-\tau) - \phi(t) - C_p\right), \\ \tfrac{d\phi}{dt} &= \alpha N(t) + \kappa \tfrac{R(t-\tau)}{R(t)}\sin\left(\phi(t-\tau) - \phi(t) - C_p\right), \\ T\tfrac{dN}{dt} &= P - N(t) - \left(1 + 2N(t)\right)R(t)^2. \end{aligned} \tag{5}$$

Inserting the ansatz (4) yields the equations

$$\begin{aligned} 0 &= N_s R_s + \kappa R_s \cos(\omega\tau + C_p) \\ \omega &= \alpha N_s - \kappa \sin(\omega\tau + C_p) \\ 0 &= P - N_s - (1 + 2N_s)R_s^2 \end{aligned} \tag{6}$$

for the constants R_s, N_s and ω. Since it is assumed that $R_s \neq 0$, these equations can be simplified to

$$\omega = -\kappa\left(\alpha\cos(\omega\tau + C_p) + \sin(\omega\tau + C_p)\right) \tag{7}$$

$$N_s = -\kappa\cos(\omega\tau + C_p) \tag{8}$$

$$R_s^2 = \frac{P - N_s}{1 + 2N_s} \tag{9}$$

for $N_s \neq -\frac{1}{2}$.

We will use both representations (6) and (7) for ω simultaneously. Both are transcendental equations and can, therefore, not be solved explicitly for ω. However, once ω has been obtained, N_s and R_s follow from (8) and (9).

From ansatz (4) it is clear that R_s must be real and positive; otherwise the solution of (7)–(9) is not physically relevant. In particular, the condition that the solution be physically relevant means that $R_s^2 > 0$ must hold, which means that from (9) we obtain a restriction on N_s, namely

$$-\frac{1}{2} < N_s \leq P \text{ for } P > -\frac{1}{2}\,. \tag{10}$$

The implication of this restriction will be studied in more detail in section 5.

4 The number of possible ECMs

We first determine the number of *possible* ECMs irrespective of conditions (10). Equation (7) can be rewritten as

$$\omega = -\frac{K}{\tau}\sin\left(\omega\tau + C_p + \arctan(\alpha)\right) \tag{11}$$

where $K = \kappa\tau\sqrt{\alpha^2+1}$ is called the effective feedback strength. The geometric interpretation of (11) is that the ECMs are given as the intersection points of a line and a sine function with amplitude $\frac{K}{\tau}$. Therefore, there is always at least one solution. When κ is increased, the amplitude of the right-hand-side increases and more ECMs are formed in pairs in saddle-node bifurcations.

We define the functions

$$f(\omega) = -\frac{K}{\tau}\sin\left(\omega\tau + C_p + \arctan(\alpha)\right)\,, \tag{12}$$

$$g(\omega) = \omega\,, \tag{13}$$

so that the intersection points of f and g correspond to ECMs. Saddle-node bifurcations where a new pair of ECMs is formed, take place at exactly those values of κ where $\frac{\partial f}{\partial \omega} = \frac{\partial g}{\partial \omega}$ and $f = g$; see Fig. 2. From the first condition, or by differentiating (11) with respect to ω, we obtain

$$\cos\left(\omega\tau + C_p + \arctan(\alpha)\right) = -\frac{1}{K} \tag{14}$$

which has solutions as long as $K \geq 1$.

Note that saddle-node bifurcations take place alternatingly where the function f is positive and negative. For the ECMs formed when $f > 0$ [Fig. 2(c)], the corresponding N_s is always positive (upon creation). However, for the branch where $f < 0$ [Fig. 2(a)] N_s varies from positive to negative as C_p (or κ) is increased.

It follows from (14) that

$$\sin\left(\omega\tau + C_p + \arctan(\alpha)\right) = \pm\frac{1}{|K|}\sqrt{K^2-1} \tag{15}$$

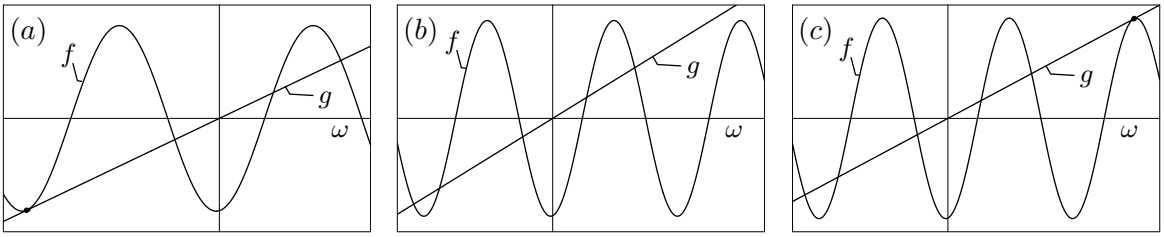

Figure 2: Plots of f and g as functions of ω. In panel (a) a new pair of ECMs is created at a saddle-node bifurcation for $f < 0$ (at a minimum of f), panel (b) is a generic situation, and in panel (c) two ECMs are formed in a saddle-node bifurcation at a point where $f > 0$ (at a maximum of f).

and also that

$$\omega\tau + C_p + \arctan(\alpha) = \pm \arccos\left(-\frac{1}{K}\right) + 2k\pi \tag{16}$$

for $k \in \mathbf{Z}$, where the sign in Eqs. (15) and (16) is the same. Substituting (15) into (11) and using (16) leads to the expression for the locus of saddle-node bifurcations

$$C_p^{S\pm}(K) = \pm\left[\sqrt{K^2-1} + \arccos\left(-\frac{1}{K}\right)\right] - \arctan(\alpha) + 2k\pi. \tag{17}$$

Note that this expression does not depend on the pump P.

For $K < 1$ no saddle-node bifurcations take place and only one ECM exists. For $K \geq 1$ we can determine the possible number of ECMs in (C_p, κ, P)-space. Since (17) does not depend on the pump current P, intersections with planes $\{P = constant\}$ all have the same structure that is given in Fig. 3; compare with [Van Tartwijk and Agrawal (1998)]. On these curves in the (C_p, κ)-plane possible ECMs are formed in pairs and we can determine their number in each of the open regions. The lowest point of the curves is a cusp point at $(\kappa^c, C_p^c) = (1/\tau\sqrt{\alpha^2+1}, \pi - \arctan\,\alpha + 2k\pi)$.

The saddle-node bifurcations take place where (14) holds, that is, when

$$\kappa\tau(\alpha\sin(\omega\tau + C_p) - \cos(\omega\tau + C_p)) = 1. \tag{18}$$

By substituting (6) and (8) we obtain an expression for the line in the (ω, N_s)-plane on which the saddle-node bifurcation takes place, namely

$$N_s = \frac{1 + \tau\alpha\omega}{\tau(\alpha^2+1)}. \tag{19}$$

Substituting the expression for ω that was obtained by combining (15) with (11), we find the explicit expressions

$$\begin{aligned} N_s^S &= \tfrac{1}{\tau(\alpha^2+1)}\left[1 \mp \alpha\sqrt{\tau^2\kappa^2(\alpha^2+1) - 1}\right], \\ \omega^S &= \mp\tfrac{1}{\tau}\sqrt{\tau^2\kappa^2(\alpha^2+1) - 1} \end{aligned} \tag{20}$$

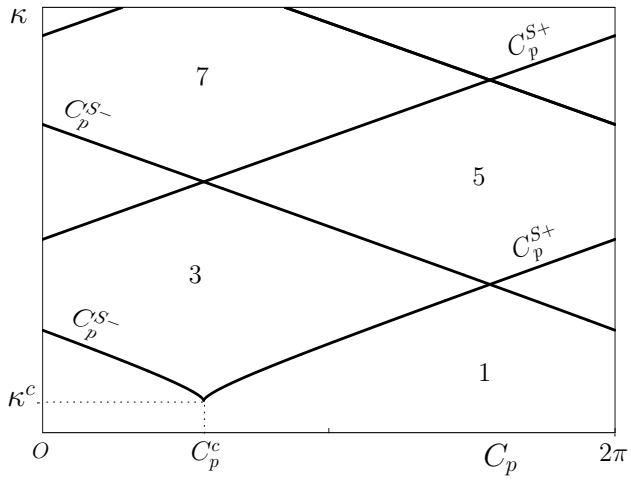

Figure 3: Regions in the (C_p, κ)-plane labeled with the number of possible ECMs; note that this image is independent of P.

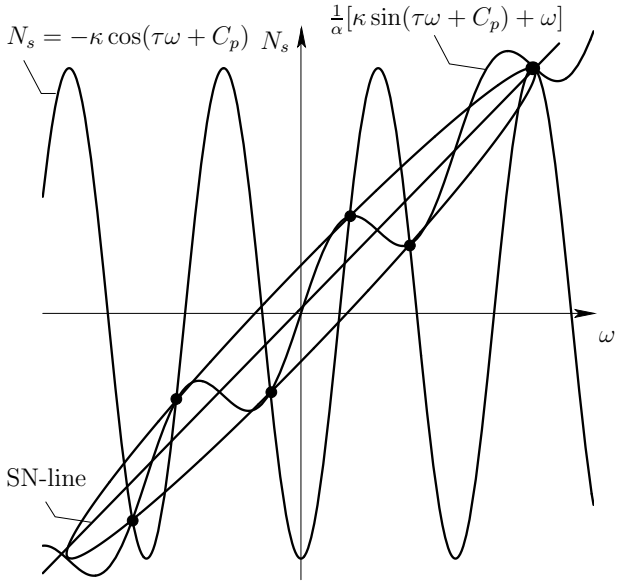

Figure 4: Plot of the ellipse (21), the graphs of equations (6) and (8), and the SN-line (19) on which the saddle-node bifurcations take place. The ECMs are the intersection points of the two curves given by (6) and (8).

while R_s can be determined from (9).

The ECMs must also satisfy

$$N_s^2 + (\omega - \alpha N_s)^2 = \kappa^2\,, \tag{21}$$

which follows from writing (6) as $\omega - \alpha N_s = -\kappa\sin(\omega\tau + C_p)$, taking the square of this equation and adding it to the square of (8). In the (ω, N_s)-plane this defines an ellipse —

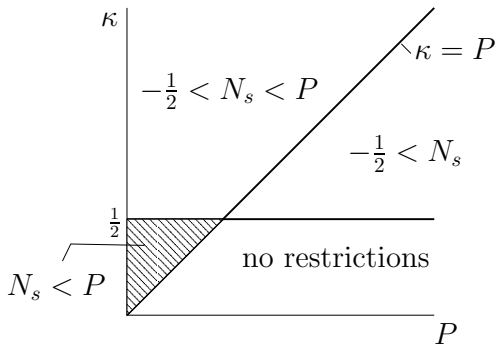

Figure 5: Illustration of regions in the (P, κ)-plane of restrictions arising from (10).

the well-known ellipse of ECMs; see, e.g., [Van Tartwijk and Agrawal (1998)]. In Fig. 4 the ellipse (21) is plotted together with the graphs of (6) and (8). Also plotted is the (diagonal) line (19) where the saddle-node bifurcation takes place. The ECMs are exactly the intersection points of the two graphs of (6) and (8), which indeed lie on the ellipse. The ECMs that lie below the SN-line (19) in Fig. 4 are often called the modes, and those above the SN-line are called the antimodes. Note that the antimodes satisfy

$$N_s > \frac{1 + \tau\alpha\omega}{\tau(\alpha^2 + 1)}\,. \tag{22}$$

5 Physically relevant ECMs

The number of possible ECMs that is shown in Fig. 3 can be achieved only for sufficiently high pump current P. Indeed it was noted earlier that ECMs may not be physical for too low pump current; see, e.g., [Gavrielides (2000), Haegeman *et al.* (2002)]. To determine the actual number of ECMs — which are referred to as physically relevant ECMs — we need to take account of the extra parameter P. Specifically, we analyze what bifurcation occurs in Eqs. (1) when ECMs become (or cease to be) physically relevant. The results constitute a bifurcation analysis in (C_p, κ, P)-space, which we present with representative sections in the (C_p, κ)-plane for different values of P.

The key realization is that one needs to take account of the two conditions of Eqs. (10), which can be split up into

$$N_s \;>\; -\frac{1}{2}\,, \tag{23}$$

$$N_s \;\leq\; P. \tag{24}$$

Conditions (23) and (24) define four different regions in the (P, κ)-plane as sketched in Fig. 5. In the region where $\kappa < \frac{1}{2}$ and $\kappa < P$, both conditions are always satisfied. However, in the other regions (23) and (24) are not always satisfied and lead to extra restrictions as shown in Fig. 5.

Since κ is assumed to be relatively small in any Lang-Kobayashi-type rate equation model, our analysis focuses on the regions below the line $\{\kappa = \frac{1}{2}\}$, specifically on the shaded region where the extra restriction (24) on N_s needs to be satisfied.

When an ECM moves closer and closer to the boundary where it ceases to be physically relevant it follows from (9) that its 'radius' R_s becomes smaller and smaller. Physically, this means that its intensity $I_s = R_s^2$ goes to zero. When the boundary is reached, the radius becomes zero, which suggests a Hopf bifurcation with a solution on the axis $\{E = 0\}$ in (E, N)-space. This can only be the basic solution discussed in Sec. 2.

To see that this is indeed the case we substitute $N_s = P$ into equation (8) and obtain the two expressions

$$\begin{aligned} \omega\tau + C_p &= \pm \arccos\Big(-\tfrac{P}{\kappa}\Big) + 2k\pi\,, \\ \sin(\omega\tau + C_p) &= \pm\sqrt{1-\cos^2(\omega\tau + C_p)} = \pm\tfrac{1}{\kappa}\sqrt{\kappa^2 - P^2}. \end{aligned} \tag{25}$$

Substituting both these equations together with $N_s = P$ into (6) gives the curves

$$C_p^{P\pm}(\kappa, P) = \pm\left[\arccos(-\frac{P}{\kappa}) + \tau\sqrt{\kappa^2 - P^2}\right] - \alpha\tau P + 2k\pi, \tag{26}$$

which is indeed exactly expression (3) for a Hopf bifurcation of the basic solution $(0, P)$. In other words, $C_p^{P\pm}(\kappa, P) = C_p^{H\pm}(\kappa, P)$.

Parametrization (26) defines a surface in (C_p, κ, P)-space where $R_s = 0$. When crossing this surface by changing the parameters, ECMs become, or cease to be, 'physically relevant'. Thus, the sketch of the possible number of ECMs given in Fig. 3 can now be completed to give the actual numbers of physically relevant ECMs.

We first present in Fig. 6 six representative cross sections, namely the (C_p, κ)-plane for fixed values of $P > 0$, that is, above the solitary laser threshold. The blue saddle-node bifurcation curve is repeated from Fig. 3. The relevant new object is the green curve of Hopf bifurcation of the basic solution, where physically relevant solutions are born or lost. This curve is tangent to the saddle-node curve at a saddle-node Hopf point (C_p^*, κ^*), which can be computed as follows. Setting $N_s = P$ in the expression (20) for the N_s-value at the saddle-node bifurcation we find that

$$\kappa^* = \sqrt{P^2 + \frac{1}{\tau^2\alpha^2}(1 - \tau P)^2}.$$

The tangency point changes the nature of the saddle-node bifurcation along the blue curve. Along the dark blue part of the curve two physically relevant ECMs are created. However, along the light blue part of the saddle-node curve two ECMs are created with $N_s > P$. Hence, these ECMs are not physically relevant since they do not satisfy condition (24).

The open regions that are bounded by the green and dark blue curves correspond to regions with different numbers of physically relevant ECMs. The green curve of Hopf bifurcation of the basic solution is split by (C_p^*, κ^*) into two parts. For both parts, the number of physically relevant ECMs increases by one when crossing the curve from left to right.

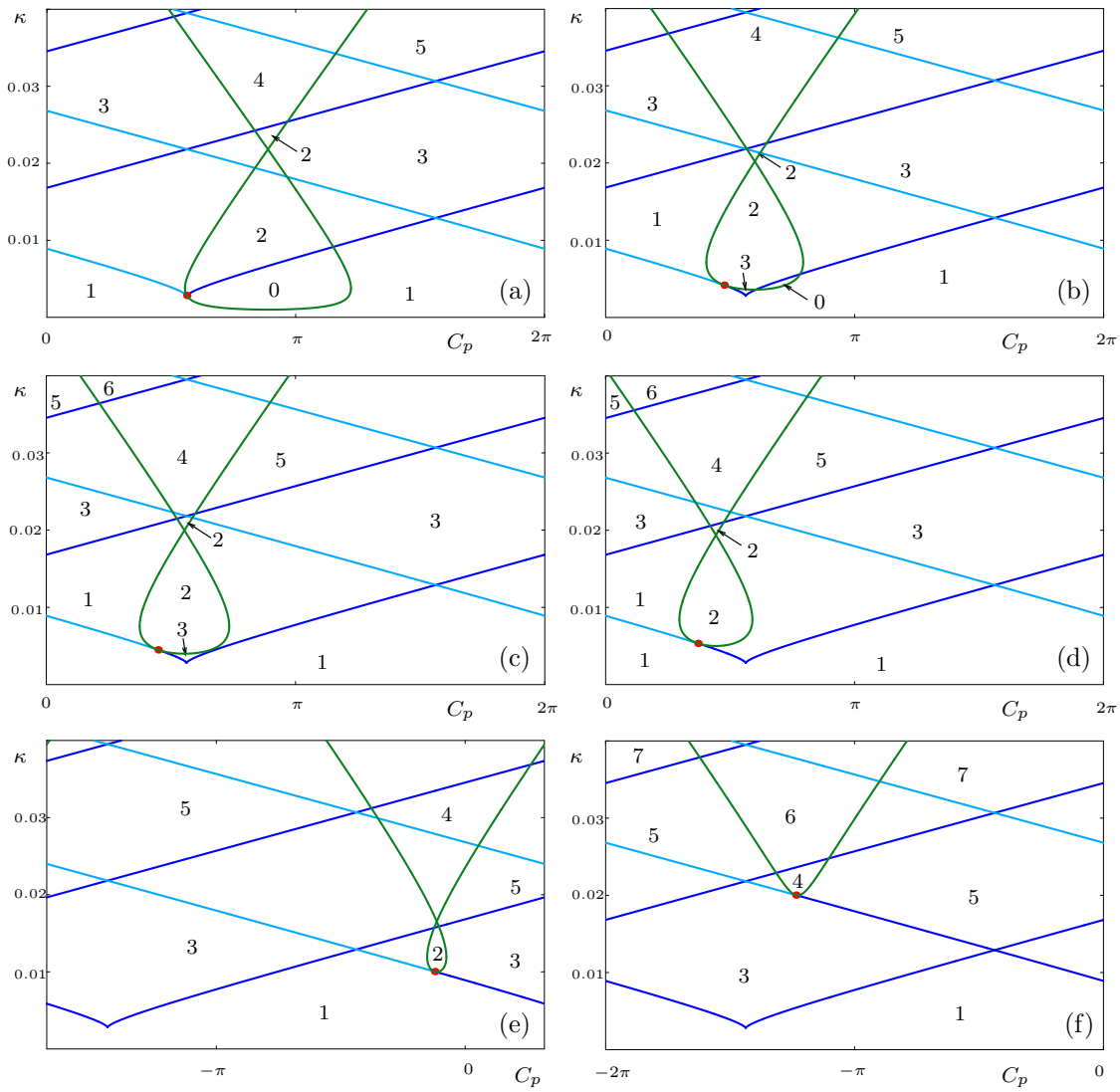

Figure 6: The bifurcation set in the (C_p, κ)-plane, where from (a) to (f) the pump current P increases through the values 0.001, 0.0036, 0.004, 0.005, 0.01, and 0.02. Shown are curves of saddle-node bifurcation (blue) and curves of Hopf bifurcation (green) of the basic solution along which physically relevant solutions bifurcate. Inside the green loop in panels (a) to (e) the off-state of the lase is stable. Along the light blue parts of the saddle-node curve the bifurcating ECMs are not physically relevant. Notice that the 2π-wide C_p-window varies in order to 'track' the green curve of Hopf bifurcations.

In particular, inside the loop formed by this curve (see Fig. 6(a)–(e)) the basic solution is stable; compare Fig. 1. Physically, the fact that the laser may actually be off above the solitary laser threshold of $P = 0$ can be interpreted as negative interference (for C_p around π) between the field in the laser and the reflected field. The laser is off in the regions labeled 0 in Fig. 6(a) and (b), but two ECMs exists in the remaining part of the

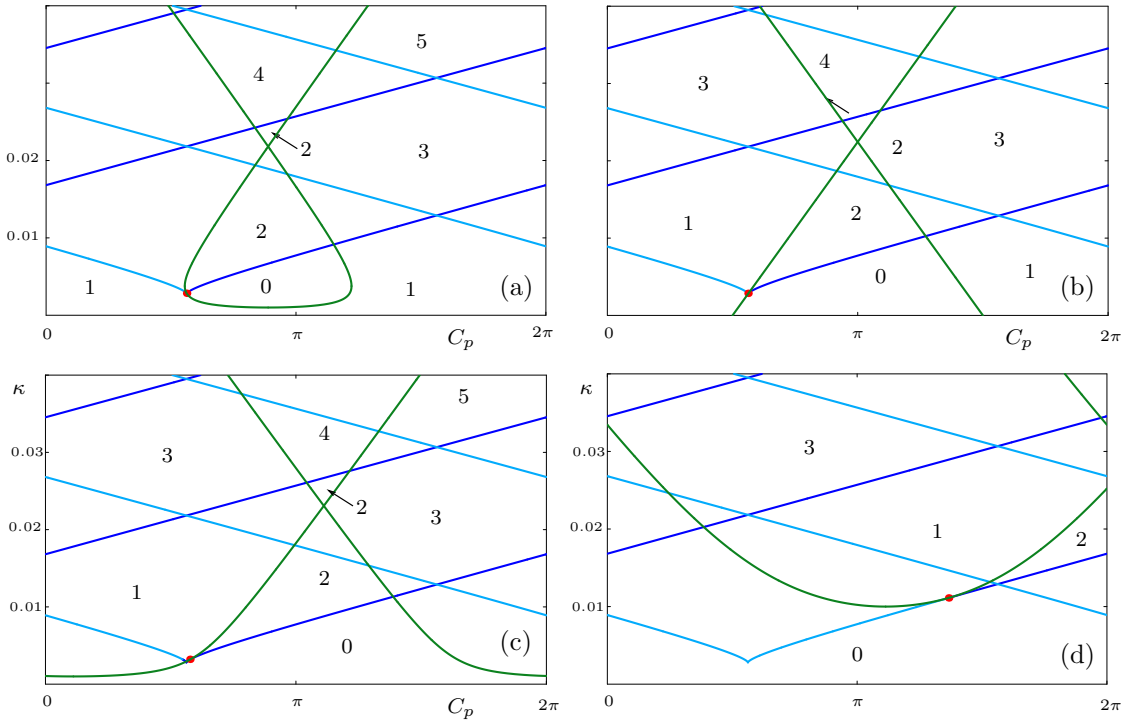

Figure 7: The bifurcation set in the (C_p, κ)-plane shown as in Fig. 6, where from (a) to (d) the pump current P now decreases through the values 0.001, 0.0, -0.001, and -0.01.

inside of the loop. In other words, there is the possibility of a bistability of the off-state with a stable ECM or more complicated stable dynamics. This is shown to be indeed the case in the stability analysis of Sec. 6.4.

Figure 6 shows clearly how the loop of the green Hopf curve becomes smaller and finally disappears. At the same time the green curve moves along the left-hand branch of the blue saddle-node curve toward higher values of κ. Eventually, it will leave the shown region of κ values altogether, so that the picture will resemble Fig. 3. From that value of the pump current P on, all possible ECMs in the region of interest will be physically relevant.

We now address the question what happens when P is decreased to below the solitary laser threshold of $P = 0$. Note that it is well known that the laser may actually be lasing even below its solitary laser threshold, because the light that is fed back may counter the losses that need to be overcome for lasing — a phenomenon known as threshold reduction; see, e.g., [Fischer et al. (2000a)]. This effect can be interpreted as positive interference between the laser field and the feedback field. Nevertheless, when the pump current P is too low one would expect the laser to be off even in the presence of optical feedback.

Figure 7 shows how this physical insight manifests itself in terms of bifurcations of ECMs in the (C_p, κ)-plane. The loop in Fig. 7(a), where $P = 0.001$, grows and become degenerate for $P = 0$ in panel (b), where it 'connects' with the line $\{\kappa = 0\}$ at $\pi/2$ and $3\pi/2$. For $P < 0$ there is a κ-value below which the laser is off irrespective of the value

of the feedback phase C_p. Nevertheless, as expected, the threshold reduction is largest near (multiples of) 2π, where a little feedback already leads to stable lasing in the region labeled 1. As P is decreased further, the green curve moves up along the right-hand blue curve until it leaves the window of κ-values. At this point, the saddle-node curve in this window will correspond entirely to bifurcations of nonphysical ECMs, so that the stable off solution is the only solution.

6 Stability of ECMs

In this section, we study the stability of the ECMs. To this end we need to compute their characteristic equation, which can be obtained by computing the linear variational equation around an ECM [Krauskopf (2005)]. Equation (1) can be written as

$$\frac{d}{dt}\begin{pmatrix} R(t) \\ \phi(t) \\ N(t) \end{pmatrix} = F(R(t), \phi(t), N(t), R(t-\tau), \phi(t-\tau))$$

where

$$F(x, y, z, v, w) = \begin{bmatrix} xz + \kappa v \cos(H) \\ \alpha z + \kappa \frac{v}{x} \sin(H) \\ \frac{1}{T}[P - z - (1+2z)x^2] \end{bmatrix}$$

and $H = w - y - C_p$. The linear variational equation around an ECM then becomes

$$\frac{d}{dt}\begin{pmatrix} R(t) \\ \phi(t) \\ N(t) \end{pmatrix} = DF(R_s, (\omega_s - \frac{C_p}{\tau})t, N_s, R_s, (\omega_s - \frac{C_p}{\tau})(t-\tau)) \begin{pmatrix} R(t) \\ \phi(t) \\ N(t) \\ R(t-\tau) \\ \phi(t-\tau) \end{pmatrix}.$$

Here DF denotes the Jacobian of F, and it is given by

$$DF(x, y, z, v, w) = \begin{bmatrix} z & \kappa v \sin(H) & x & \kappa \cos(H) & -\kappa v \sin(H) \\ -\kappa \frac{v}{x^2} \sin(H) & -\kappa \frac{v}{x} \cos(H) & \alpha & \frac{\kappa}{x} \sin(H) & \kappa \frac{v}{x} \cos(H) \\ -\frac{2x}{T}(1+2z) & 0 & -\frac{1}{T}(2x^2+1) & 0 & 0 \end{bmatrix}.$$

This equation can also be written as

$$\frac{dx(t)}{dt} = Ax(t) + Bx(t-\tau); \quad x(t) = \begin{pmatrix} R(t) \\ \phi(t) \\ N(t) \end{pmatrix}$$

with

$$A = \begin{bmatrix} N_s & -\kappa R_s \sin(\omega_s \tau) & R_s \\ \frac{\kappa}{R_s} \sin(\omega_s \tau) & -\kappa \cos(\omega_s \tau) & \alpha \\ -\frac{2}{T}(1+2N_s)R_s & 0 & -\frac{1}{T}(1+2R_s^2) \end{bmatrix} \tag{27}$$

and

$$B = \begin{bmatrix} -\kappa\cos(\omega_s\tau) & \kappa R_s\sin(\omega_s\tau) & 0 \\ -\frac{\kappa}{R_s}\sin(\omega_s\tau) & \kappa\cos(\omega_s\tau) & 0 \\ 0 & 0 & 0 \end{bmatrix}. \tag{28}$$

The characteristic equation is then given by

$$\det\Delta(\lambda) = 0 \text{ where } \Delta(\lambda) = \lambda I - A - e^{-\lambda\tau}B. \tag{29}$$

After an extended calculation this leads to the characteristic equation

$$\begin{aligned} &\lambda^3 + \lambda^2[\tfrac{1}{T}(1+2R_s^2) - 2N_s(1-e^{-\lambda\tau})] + \lambda[\tfrac{2R_s^2}{T}(1+2N_s) + \kappa^2(1-e^{-\lambda\tau})^2 \\ &+\tfrac{2\kappa}{T}\cos(\omega_s\tau)(1+2R_s^2)(1-e^{-\lambda\tau})] + \tfrac{\kappa^2}{T}(1+2R_s^2)(1-e^{-\lambda\tau})^2 \\ &+\tfrac{2\kappa R_s^2}{T}(1+2N_s)(1-e^{-\lambda\tau})(\cos(\omega_s\tau) - \alpha\sin(\omega_s\tau)) = 0\,. \end{aligned} \tag{30}$$

Since (1) is a delay equation this characteristic equation is transcendental and has infinitely many solutions, called the characteristic roots.

In numerical simulations it can be found that the ECMs for which $\kappa\tau(\alpha\sin(\omega_s\tau) - \cos(\omega_s\tau)) < 1$ are stable upon creation and then lose their stability in a Hopf bifurcation as κ increases. However, from (30) this can not be concluded easily.

It is quite a challenge to extract similar analytical information about the stability of the ECMs from (30). The approach we take here is to consider the stability for special sets of ECMs, such as those that exist close to certain bifurcation curves. In particular, we also take into account that there are parameter regions where the solutions are not physically relevant.

Recall that in section 2, we already analysed the stability of the basis solution $(0, P)$. Here, we study the stability of the ECMs on the curves $C_p^{H\pm} = C_p^{P\pm}$ where this basic solution undergoes a Hopf bifurcation.

6.1 The stability of the solution that can be continued from the solitary laser solution

In section 4, we found that one ECM is formed when κ is increased from $\kappa = 0$, and that this ECM exists for all $\kappa > 0$, although there are regions where it is not physically relevant. This is the solution that can be continued from the solitary laser solution for $\kappa > 0$ and we will denote this solution by ECM^S.

We can determine the stability of ECM^S, under the extra condition that it is physically relevant, for $\kappa \ll 1$. For $\kappa \ll 1$, ECM^S is a small perturbation of the solution for $\kappa = 0$: $N_s = 0, \omega_s = \omega_0$ and $R_s^2 = P$ and, its eigenvalues are small perturbations of the eigenvalues of this solution. Therefore, we first determine the eigenvalues for the solution for $\kappa = 0$. For $\kappa = 0$, the LK-equations reduce to ODEs and there are finitely many eigenvalues that can be determined explicitly as

$$\lambda = 0, \quad \lambda_\pm = \frac{1}{2T}\left[-(1+2P) \pm \sqrt{(1+2P)^2 - 8PT}\right].$$

From this we find that $\mathrm{Re}(\lambda_\pm) < 0$ for $P, T > 0$.

Upon setting κ nonzero these eigenvalues change with a small perturbation and for all eigenvalues λ, one finds that $\mathrm{Re}(\lambda) < 0$ still holds for $\kappa \ll 1$ as long as $\kappa \ll P, \frac{1}{T}$. Hence ECM^S is stable when it is created in $\kappa = 0$, and physically relevant, and it remains stable until it undergoes a Hopf-bifurcation.

In section 6.3, we will study the stability of ECM^S on the curves where the physical relevance changes. There, we determine where it undergoes a Hopf-bifurcation such that it becomes unstable.

6.2 Anti-modes near the saddle-node bifurcation

We know that the ECMs are formed in saddle-node bifurcations and, therefore, upon creation, one of the ECMs of such a pair has one unstable eigendirection *more* than the other ECM. Hence this ECM is unstable upon creation. However, since the equations are studied in an infinitely dimensional phase-space this does not imply that the other ECM of the pair is stable.

Using (30) we now prove that the ECMs above the line (19) where the SN bifurcation takes place, the 'antimodes', are those solutions with at least one eigenvalue with positive real part. Therefore these ECMs are unstable for every choice of κ.

We assume that $|\lambda\tau| \ll 1$ and will make use of the fact that $\kappa\tau(\alpha\sin(\omega_s\tau) - \cos(\omega_s\tau)) > 1$. Then, the exponential term in (30) can be expanded as $1 - e^{-\lambda\tau} = \lambda\tau + \mathcal{O}((\lambda\tau)^2)$ and the characteristic equation reduces to

$$\begin{aligned}\lambda[\lambda^2(1 - 2N_s\tau + \kappa^2\tau^2) + \lambda\tfrac{1+2P}{T(1+2N_s)}(1 - 2N_s\tau + \kappa^2\tau^2) \\ + \tfrac{2(P-N_s)}{T}(1 + \kappa\tau(\cos(\omega_s\tau) - \alpha\sin(\omega_s\tau)))] = 0. \end{aligned} \tag{31}$$

This equation can be solved explicitly and has the solutions

$$\lambda = 0, \quad \lambda_\pm = -\frac{1+2P}{T(1+2N_s)} \pm \frac{1}{2}\sqrt{D}$$

where

$$D = (\frac{1+2P}{2T(1+2N_s)})^2 - 8\frac{(P-N_s)}{T(1 - 2N_s\tau + \kappa^2\tau^2)}(1 + \kappa\tau(\cos(\omega_s\tau) - \alpha\sin(\omega_s\tau)).$$

Since $-\kappa < N_s < \kappa$ (from (8)) and $\tau > 0$ it follows that $1 - 2N_s\tau + \kappa^2\tau^2 > 0$. When assuming that $\kappa\tau(\alpha\sin(\omega_s\tau) - \cos(\omega_s\tau)) > 1$ we find that

$$D > (\frac{1+2P}{T(1+2N_s)})^2,$$

where we also use that $N_s < P$. This implies that $\lambda_+ > 0$ and hence these ECMs, the 'anti-modes', are all unstable when they are formed in the SN-bifurcation.

6.3 Stability on the curve of changing physical relevance

In this section we determine the stability of the ECM that (dis)appears on the curve $C_p^{P\pm}(\kappa, P)$, given by (26). Along this curve an ECM becomes, or ceases to be, physically relevant in a Hopf bifurcation of the basic solution $(0, P)$. On this curve the characteristic equation reduces considerably since $R_s = 0$ and $N_s = P$. We find the characteristic root $\lambda = -\frac{1}{T}$, and the other solutions of (30) must satisfy

$$\lambda = [P \pm i\sqrt{\kappa^2 - P^2}](1 - e^{-\lambda\tau}) \tag{32}$$

since $\kappa \geq P$ on $C_p^{P\pm}(\kappa, P)$.

For the lowest point on the curve where $\kappa = P$ we can study the sign of the real part of the eigenvalues. Introducing $\kappa = P$ into (32) leads to

$$\lambda = P(1 - e^{-\lambda\tau}).$$

If we change to a new variable $z = \tau\lambda$ and then set $z = \nu + i\mu$ we obtain

$$\begin{aligned} \nu &= \tau P(1 - e^{-\nu}\cos\mu) \\ e^{\nu}\mu &= \tau P \sin\mu. \end{aligned}$$

If we assume that there exists an eigenvalue with Re $(\lambda) > 0$ so that the ECM would be unstable some careful analysis yields that *only* for $P > \frac{1}{\tau}$ there does indeed exist such a λ with Re $(\lambda) > 0$ for the ECMs and, for $0 < P < \frac{1}{\tau}$ Re $(\lambda) < 0$ for all λ.

Hence, the ECM that disappears at $\kappa = P$ is unstable for $P > \frac{1}{\tau}$. On the other hand, for $0 < P < \frac{1}{\tau}$ the ECM that disappears at $\kappa = P$ is stable.

We now study the eigenvalues on the rest of the curve $C_p^{P\pm}(\kappa, P)$, that is, for $\kappa \neq P$. Using (32), substituting $\lambda = i\mu$ and splitting into real and complex parts yields (after eliminating μ) that a Hopf bifurcation of the ECMs takes place at those points on the curve where

$$\arccos(\frac{P}{\tau\kappa^2}) + 2l\pi = \sqrt{\frac{\tau^2\kappa^4}{P^2} - 1}, \quad l \in \mathbf{Z} \tag{33}$$

is satisfied. As κ is increased along $C_p^{P\pm}(\kappa, P)$ from $\kappa = P$ (the lowest point), the first Hopf bifurcation takes place when $\kappa_{hopf}^2 = \frac{P}{\tau}$ (here $l = 0$). Note that this point only lies on $C_p^{P\pm}(\kappa, P)$ for $P < \frac{1}{\tau}$ because only then it satisfies $\kappa > P$. By contrast, in the case that $P > \frac{1}{\tau}$, we found above that the ECM is already unstable at $\kappa = P$ and, hence, these Hopf bifurcation points are less important.

Summarising, for $P < \frac{1}{\tau}$ the ECM on $C_p^{P\pm}(\kappa, P)$ is stable for $\kappa = P$. At $\kappa_{hopf} = \sqrt{\frac{P}{\tau}}$ a Hopf bifurcation takes place, creating an eigenvalue λ with $\mathrm{Re}(\lambda) > 0$ and, hence, the ECMs created for $\kappa_{hopf} > \sqrt{\frac{P}{\tau}}$ are unstable. For $P > \frac{1}{\tau}$, the ECM is unstable everywhere when it disappears on $C_p^{P\pm}(\kappa, P)$.

Before we continue to study what these results imply, we analyse the relation between κ_{hopf} and κ^*. Recall that at κ^*, the saddle-node curves $C_p^{S\pm}$ and the curve $C_p^{P\pm}(\kappa, P)$ touch and, that $C_p^{P\pm}(\kappa, P)$ is split into two parts by κ^*. We find that $\kappa_{hopf} < \kappa^*$ for $0 < P < \frac{1}{\tau(\alpha^2+1)}$, when $P = \frac{1}{\tau(\alpha^2+1)}$ and $\kappa_{hopf} > \kappa^*$ for $\frac{1}{\tau(\alpha^2+1)} < P < \frac{1}{\tau}$. For $\kappa_c = \frac{1}{\tau\sqrt{\alpha^2+1}}$

the two points κ_{hopf} and κ^* coincide. At this point $\kappa_{hopf} = \kappa^*$ the curve $C_p^{P\pm}$ has a vertical tangent, that is, $\frac{\partial C_p^{P\pm}}{\partial \kappa} = 0$.

In the next section we extend the results for ECMs on the planes $C_p^{P\pm}(\kappa, P)$ (for any C_p) to a larger part of the (C_p, κ, P)-space. In order to interpret the above results correctly it is important to know what type of ECM disappears on these planes, namely whether it is a mode, an antimode or ECM^S. Indeed, different parts of $C_p^{P\pm}(\kappa, P)$ correspond to the disappearance of different types of ECMs. This is important since we know that the antimodes are already unstable upon creation in the SN-bifurcation.

Considering the positions of the ECMs on the ellipse as given by (18) leads to the following results for the type of the ECM on the curve $C_p^{P\pm}$. On the part of curve $C_p^{P\pm}$ for which $C_p < C_p^*$ in a neighbourhood of κ^*, it is an antimode. On the part of curve $C_p^{P\pm}$ for which $C_p > C_p^*$ in a neighbourhood of κ^*, it is either a mode or ECM^S. For $C_p < C_p^c$ it is a mode and for $C_p > C_p^c$ it is ECM^S.

6.4 Stability close to the curve of changing physical relevance

Using all the above obtained information, we can now sketch the curve $C_p^{P\pm}$ with an extra colour-coding to keep track of the type of the ECM that is formed. In Fig. 8, we plot the saddle-node curves $C_p^{S\pm}$ (blue) and the curve $C_p^{P\pm}(\kappa, P)$ where ECMs disappear (green) in the (C_p, κ)-plane for various choices of P after fixing the other coefficients. The general picture will remain similar for other choices of the coefficients. The points where $\kappa = \kappa^*$ and $\kappa = \kappa_{Hopf}$ are given in black and red, respectively.

The curve $C_p^{P\pm}(\kappa, P)$ splits into several parts by taking into account the type of the ECM that disappears. On the part for which $C_p < C_p^*$ close to κ^*, the black dashed curve, the antimode disappears. Since the antimode is unstable upon creation, it remains unstable for all κ, this curve is dashed to indicate this. On the rest of $C_p^{P\pm}$, either a mode or ECM^S disappears. The mode disappears for $C_p < C_p^c$ along the dark green curve. For $C_p > C_p^c$, ECM^S disappears, and this happens along the light green part of the curve. In the figure only those values of the parameters are chosen where $0 < P < \frac{1}{\tau}$ (some of the ECM on $C_p^{P\pm}$ are indeed stable; when $P > \frac{1}{\tau}$ all the ECMs are unstable) and $\kappa_{Hopf} > \kappa^*$.

Moreover, we know that a Hopf-bifurcation takes place at κ_{Hopf} and, hence, for $\kappa > \kappa_{Hopf}$ the corresponding ECM that disappears is unstable. In Fig. 8 this is denoted by dashing the dark and light green curves for $\kappa > \kappa_{Hopf}$.

We can now continue through the point on $C_p^{P\pm}$ where $\kappa = \kappa_{Hopf}$ and conclude that a curve must exist where a Hopf-bifurcation of the ECMs takes place. This curve will extend continuously from the points on $C_p^{P\pm}$ where $\kappa = \kappa_{Hopf}$ into the (C_p, κ)-plane, tangent to $C_p^{P\pm}$.

The information about the stability of the ECMs on the curve $C_p^{P\pm}$ can be extended into regions in the (C_p, κ)-plane by using the number of ECMs in the regions. We use the fact that the stability of the mode and ECM^S does not change when κ is decreased after starting on $C_p^{P\pm}$. This is true if no other ECMs are formed in a saddle-node bifurcation in this process (when choosing κ 'between' $C_p^{S\pm}$ and $C_p^{P\pm}$) as in the case in the given plots.

From Fig. 8 (a)–(c), we can conclude that for $C_p^* < C_p < C_p^c$ the mode is stable upon creation in the saddle-node bifurcation. It remains stable until κ is slightly above $C_p^{P\pm}$

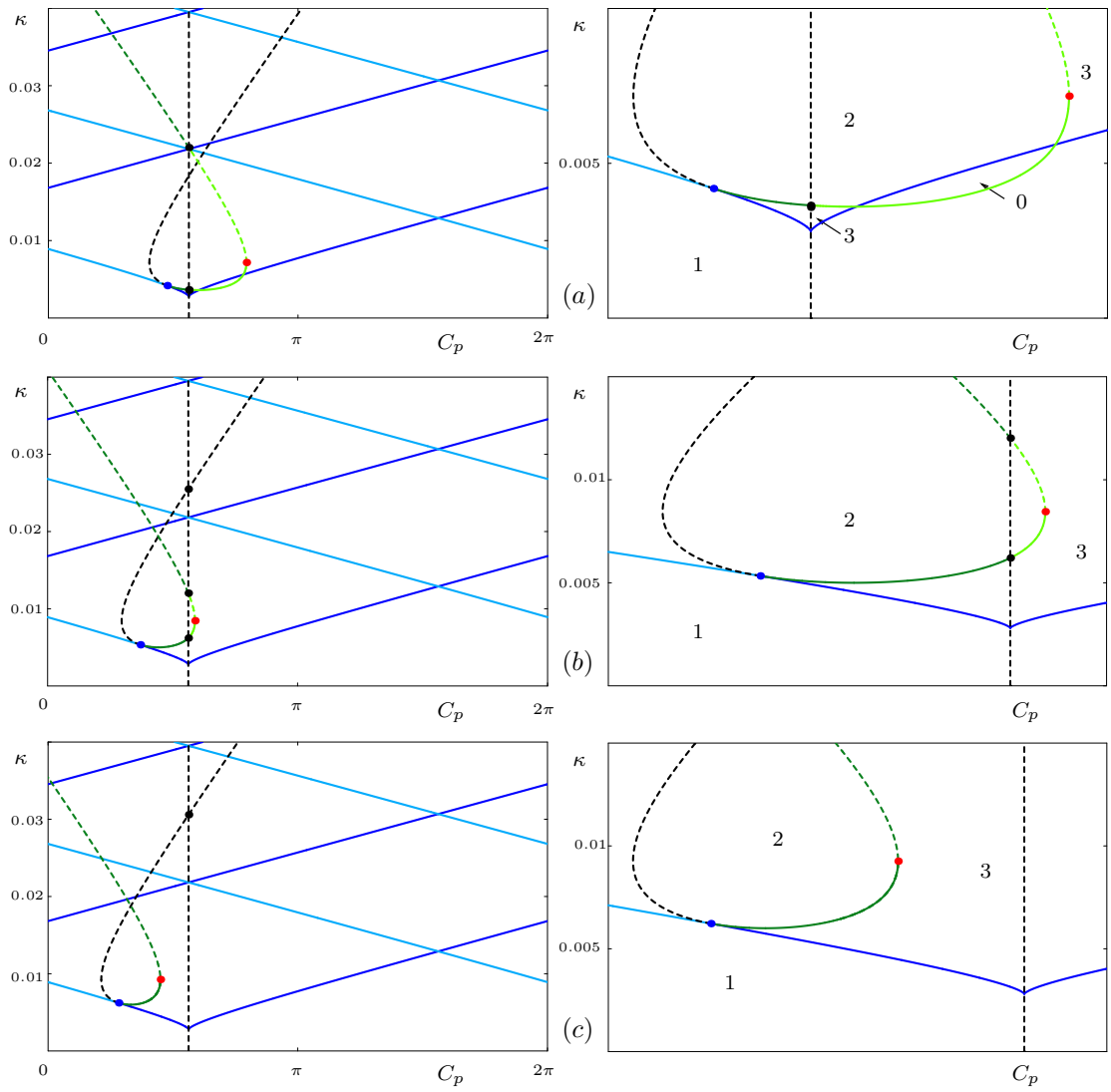

Figure 8: A plot of the saddle-node curves $C_p^{S\pm}$ (blue) where the ECMs are formed and the curves $C_p^{P\pm}$ in the (κ, C_p)-plane for the shown three values of P. On $C_p^{P\pm}$ extra colours are used to distinguish the type of ECM that disappears: on the dark green part it is the mode, on the black part the antimode, and on the light green part it is ECM^S. The dashing denotes that the ECM is unstable. The points (C_p^*, κ^*) and $\kappa = \kappa_{hopf}$ on $C_p^{P\pm}$ are shown in blue and red, respectively. In the left panel one period of C_p is shown and the right panel is an enlargement of the most interesting domain.

where it undergoes a Hopf-bifurcation. Also from Fig. 8 (a) and (b) we conclude that for $C_p > C_p^c$ the solution ECM^S is stable when increasing κ from 0 up to a region within the physical relevant loop. This is true apart from the region labelled 0 in Fig. 8 (a), where no ECM is physically relevant and where the basic solution $(0, P)$ is stable. Due to continuity there is a region of bistability between the basic solution (the off state) and

an ECM above the blue saddle-node bifurcation curve inside the loops in Fig. 8. After the Hopf bifurcation (this Hopf curve is not shown in the figure) there is a region of bistability between off state and periodic power oscillations associated with a bifurcating stable periodic orbit.

7 Conclusions

We gave a geometric picture of the backbone of physically relevant external cavity modes in the Lang-Kobayashi model of a semiconductor laser with conventional optical feedback. This was presented as two-dimensional bifurcation diagrams in the (C_p, κ)-plane for representative values of the pump current P. In this way, it is possible to show which of all possible ECMs are actually physically relevant, that is, available to the system. Of key importance is the curve of Hopf bifurcation of the basic equilibrium, which we showed acts as the threshold of individual ECMs. We identified a scenario that ties in well with what is know physically about the system, especially in terms of the role of threshold reduction near the solitary laser threshold $P = 0$.

We performed a partial stability analysis of the ECMs by means of studying the transcendental characteristic equation. Specifically, we restricted our stability calculations to the saddle-node curve and to the curve where ECMS become physically relevant, which allowed us to obtain simpler analytical formulas. We then extended these results to the regions near these special curves by a perturbation argument.

A full stability analysis in all parameters would require a detailed understanding of the complicated transcendental characteristic equation without making use of special relationships between parameters. This remains quite a challenge beyond the scope of this paper. An alternative way forward would be to make use of numerical methods to determine the stability of ECMs. One approach would be to use continuation methods, for example, the package AUTO [Doedel *et al.* 1997], to follow the locus of Hopf bifurcations as defined by the characteristic equation. Alternatively, one could apply continuation tools directly to the full DDE, such as the package DDE-BIFTOOL [Engelborghs *et al.* 1997] which also allows one to study directly the bifurcating periodic orbits and their further bifurcations.

8 Acknowledgments

The work of V.R. was supported by the Royal Dutch Academy of Sciences, and that of B.K. by an EPSRC Advanced Research Fellowship.

References

[Diekmann *et al.* 1995] O. Diekmann, S. A. Van Gils, S. M. Verduyn Lunel, and H. O. Walther. *Delay Equations: Functional-, Complex-, and Nonlinear Analysis*. Springer-Verlag, New York, 1995.

[Doedel *et al.* 1997] E. Doedel, A. Champneys, T. Fairgrieve, Y. Kuznetsov, B. Sandstede, and X. Wang. *AUTO 97: Continuation and bifurcation software for ordinary differential equations*. 1997. (`http://indy.cs.concordia.ca/auto/main.html`)

[Engelborghs *et al.* 1997] K. Engelborghs, T. Luzyanina, and G. Samaey. *DDE-BIFTOOL v2.00: a Matlab package for bifurcation analysis of delay differential equations*. Tech. Rep. TW-330, Department of Computer Science, Katholieke Universiteit Leuven, Belguim, 2000. (`http://www.cs.kuleuven.ac.be/~koen/delay/ddebiftool.shtml`)

[Fischer et al. (2000a)] I. Fischer, T. Heil, and W. Elsäßer. Emission dynamics of semiconductor lasers subject to delayed optical feedback. in [Krauskopf and Lenstra (2005)] pp 218–237.

[Fischer et al. (2000b)] I. Fischer, Y. Liu, P. Davis. Synchronization of chaotic semiconductor laser dynamics on subnanosecond time scales and its potential for chaos communication. *Phys. Rev. A* **62**:011801, 2000.

[Gavrielides (2000)] A. Gavrielides. Nonlinear dynamics of semiconductor lasers: theory and experiment. in [Krauskopf and Lenstra (2005)] pp 191–217.

[Haegeman *et al.* (2002)] B. Haegeman, K. Engelborghs, D. Roose, D. Pieroux, and T. Erneux. Stability and rupture of bifurcation bridges in semiconductor lasers subject to optical feedback. *Phys. Rev. E* **66**:046216, 2002.

[Hale and Verduyn Lunel (1993)] J. K. Hale and S. M. Verduyn Lunel. *Introduction to Functional Differential Equations*. Springer-Verlag, New York, 1993.

[Heil *et al.* (2003)] T. Heil, I. Fischer, W. Elsäßer, B. Krauskopf, K. Green, and A. Gavrielides. Delay dynamics of semiconductor lasers with short external cavities: bifurcation scenarios and mechanisms. *Phys. Rev. E* **67(6)**:066214, 2003.

[Kane and Shore (2005)] D.M. Kane and K.A. Shore (Eds.) *Unlocking Dynamical Diversity: Optical Feedback Effects on Semiconductor Lasers*. Wiley, 2005.

[Krauskopf (2005)] B. Krauskopf. Bifurcation analysis of lasers with delay. in [Kane and Shore (2005)] pp 147–183.

[Krauskopf and Lenstra (2005)] B. Krauskopf and D. Lenstra (Eds.) *Fundamental Issues of Nonlinear Laser Dynamics*. AIP Conference Proceedings 548. American Institute of Physics Publishing, Melville (New York), 2000.

[Krauskopf *et al.* (2000)] B. Krauskopf, G. H. M. Van Tartwijk, and G. R. Gray. Symmetry properties of lasers subject to optical feedback. *Opt. Commun.* **177**:347–353, 2000.

[Lang and Kobayashi (1980)] R. Lang and K. Kobayashi. External optical feedback effects on semiconductor injection laser properties. *IEEE J. Quantum Electron.* **16**: 347–355, 1980.

[Lenstra *et al.* (2005)] D. Lenstra, G. Vemuri and M. Yousefi. Generalized Optical Feedback: Theory. in [Kane and Shore (2005)] pp. 55–80

[Mørk *et al.* (1992)] J. Mørk, B. Tromborg, and J. Mark. Chaos in semiconductor lasers with optical feedback: Theory and experiment. *IEEE J. Quantum Elec.* **28**:93–107, 1992

[Ohtsubo and Davis (2005)] J. Ohtsubo and P. Davis. Chaotic Optical Communication. in [Kane and Shore (2005)] pp. 307–334.

[Van Tartwijk and Agrawal (1998)] G.H.M. Van Tartwijk and G.P. Agrawal. Laser instabilities: a modern perspective. *Prog. Quantum Electron.* **22**:43–122, 1998.

[Van Wiggeren and Roy (2002)] G. D. Van Wiggeren and R. Roy. Communication with chaotic lasers. *Science* **279**:1198–1200,1998.

[Verduyn Lunel and Krauskopf (2000)] S.M. Verduyn Lunel and B. Krauskopf. The mathematics of delay equations with an application to the Lang-Kobayashi equations. in [Kane and Shore (2005)] pp 66–86.